Desalination and Water Treatment
www.deswater.com

doi: 10.5004/dwt.2019.23714

150 (2019) 339–347
May

Functionalization of persimmon tannin with chitosan for the removal of cationic and anionic dyes from aqueous solutions

Zhongmin Wang[a], Jinliang Ning[a], Chengxian Yang[a], Xiaojuan Li[a], Mingmin Gao[a], Guiyin Li[b,]*, Zhide Zhou[b,]*

[a]*School of Materials Science and Engineering, Guilin University of Electronic Technology, Guilin, 541004, China, Tel. +86 773 2291956; emails: zmwang@guet.edu.cn (Z. Wang), ningjlde@126.com (J. Ning), YChengxian0@163.com (C. Yang), lxj42168@163.com (X. Li), gmm520530@163.com (M. Gao)*

[b]*School of Life and Environmental Sciences, Guilin University of Electronic Technology, Guilin, Guangxi, 541004, China, Tel. +86 773 2217609; emails: liguiyin01@163.com (G. Li), zzdlgy@163.com (Z. Zhou)*

Received 16 August 2018; Accepted 28 December 2018

ABSTRACT

The pollution of wastewater by dyes has aroused widespread public concern due to the potential risk to human health. Thus, we herein report the preparation of a novel bio-adsorbent (PTCS) by the functionalization persimmon tannin (PT) with chitosan (CS). The adsorption behavior of this bio-adsorbent toward dyes such as methylene blue (MB), methyl orange (MO), and rhodamine B (RB) in aqueous solutions was investigated. More specifically, the PTCS was characterized both before and after dyes adsorption using Fourier transform infrared spectroscopy (FT-IR), scanning electron microscopy (SEM), and X-ray photoelectron spectroscopy (XPS). Adsorption parameters including the pH value, bio-adsorbent dosage, initial dye concentration, and contact time were optimized, and the maximum adsorption capacities of 173.04, 60.01, and 71.06 mg/g were achieved for MB, MO, and RB, respectively. The adsorption of MO onto PTCS was found to obey the Langmuir equilibrium isotherm, while the Freundlich model better described for the adsorption of MB and RB. The adsorption kinetics for the adsorption of MO and MB fitted best with a pseudo-second-order equation, while the pseudo-first-order model was more appropriate for describing the adsorption of RB. These results indicated that the PTCS bio-adsorbent could be employed as a low-cost alternative to the treatment of dye wastewater, and so broaden the potential applications of PT in environmental research.

Keywords: Persimmon tannin; Methylene blue; Methyl orange; Rhodamine B; Adsorption

1. Introduction

Due to the rapid development of various industries worldwide, the use of dyes has become abundant in a number of areas. For example, common dyes such as methylene blue (MB), methyl orange (MO), and rhodamine B (RB) are used in the food, paper, textile, plastic, and leather industries. These industries produced large amounts of dye wastewater every year, which is particularly undesirable due to the high biological toxicities and recalcitrant entities of these dyes, in addition to their carcinogenic, teratogenic, and mutagenic properties in living organisms [1]. Therefore, the treatment of the dye wastewater is necessary prior to discharge into waterways [2,3]. However, as the majority of these dyes are stable to light and heat, they cannot be easily removed by conventional treatment methods due to their complex structures and synthetic origin. This results in deterioration in water quality, which in turn has an impact on aquatic animals and plants in addition to disrupting the ecological balance of the water [4,5]. As such, the removal of dye pollutants has become a hot

* Corresponding authors.

topic in the area of environmental science and technology. Indeed, a number of techniques have been applied for the removal of dyes from wastewater, including adsorption, coagulation precipitation, extraction, membrane separation, oxidation, and biochemical methods [6]. Among these techniques, adsorption has received the greatest amount of attention due to its simple operation, high efficiency, and low cost.

Persimmon tannin (PT), which is produced from persimmon extract and contains multiple adjacent phenolic hydroxyl groups, is an inexpensive and abundant natural biomass product that has been employed as a promising and efficient adsorbent for the selective binding and recovery of metal ions [7]. However, due to its high solubility in water, PT must be chemically modified or immobilized onto water-insoluble matrixes to increase its adsorption capacity as an efficient adsorbent in aqueous media [8]. To date, a number of attempts have been made to immobilize PT onto various water-insoluble matrixes (e.g., cellulose, SiO_2, and graphene oxide) [9–11]. Indeed, various PT-based bio-adsorbents and subsequent investigations into their adsorption characteristics toward metal cations and dyes in aqueous solutions have previously reported [12–14]. For example, Zhou et al., [12] employed chitosan-functionalized PT for the absorption of Pd(II) with a maximum adsorption capacity of 330 mg/g. Li et al., [13] utilized graphene oxide-functionalized PT to absorb precious metals, such as Au^{3+}, Pd^{2+}, and Ag^{+} ions. Also, Li et al., [14] prepared a novel and recyclable bio-adsorbent (PTP) by the cationization of PT with polyethyleneimine for the removal of the anionic dye MO from aqueous solution with maximum adsorption capacity of 225.74 mg/g.

Herein, we reported the use of PTCS as an efficient bio-adsorbent for the removal of cationic dyes (RB, MB) and anionic dye (MO) from aqueous media. The PTCS has been prepared by the chitosan (CS) surface-modification of PT through glutaraldehyde cross-linking reaction, as reported in our previous study [12]. Compared with the previously reported synthesis methods of tannin-based composites, CS used to modify the PT is a natural biomass material originating from shrimp and crab shells and is nontoxic, biodegradable, and biocompatible [8]. CS contains rich amino ($-NH_2$) and hydroxyl (-OH), which can react with pollutants such as heavy metals and dyes [16–18]. Therefore, functionalizing of PT with CS to obtain the PTCS bio-adsorbent with better performance to remove dyes, and it doesn't pollute the water. Furthermore, compared with other dye adsorbents [19–21], CS is cheaper and biocompatibility, the synthesis of PTCS can not only obtain biological adsorbent with high adsorption performance, but also greatly reduce human and raw material costs. In addition, the adsorption equilibrium, kinetics, and thermodynamics behaviors for PTCS adsorption toward dyes (MB, MO, and RB) have comprehensively been investigated. The PTCS bio-adsorbent was characterized both before and after dye adsorption with Fourier transform infrared spectroscopy (FT-IR), scanning electron microscopy (SEM), and X-ray photoelectron spectroscopy (XPS), and the adsorption mechanism was explored. Finally, the simulated wastewater treatment and recyclability of PTCS for dyes was evaluated.

2. Experimental setup

2.1. Materials and reagents

PT was donated by the Guangxi Huikun Company of Agricultural Products (Guangxi, China). CS, glutaraldehyde (50%), MB, MO, and RB were purchased from Guilin Beier Laboratory Equipment Company (Guangxi, China). All chemicals were of analytical grade and were used without further purification. Ultrapure water (18 MΩ) was obtained from a Milli-Q purification system (Milli-Pore, Bedford, MA, USA).

2.2. Preparation of PTCS by functionalizing of Persimmon tannin with Chitosan

The PTCS was prepared via a glutaraldehyde cross-linking reaction using CS and PT, as described in our previous study with minor modifications [12]. Briefly, PT (10 g) was dissolved in ultrapure water (300 mL) and mixed with CS (5 g) at pH 7.0. The resulting mixture was stirred at 303 K for 8 h, after which time the suspended matter was filtered and washed with distilled water. Glutaraldehyde (25 mL) was then added to the suspended matter, and the mixture was stirred at 298 K for 4 h then at 313 K for 4 h. Finally, the obtained product was washed with distilled water and filtered. The filter cake was dried under vacuum at 313 K over 24 h, and the dried PTCS product was crushed and sieved into uniform particles (≤200 nm diameter).

2.3. Effect of the initial pH on the adsorption capacity

PTCS (15 mg) was added to solutions of MB (20 mg/L, 100 mL), MO (20 mg/L, 100 mL), RB (20 mg/L, 100 mL) with initial pH values of 2, 4, 6, 8, 10, and 12, respectively. The pH of the initial solution was adjusted using either a 0.1 mol/L HCl solution or a 0.1 mol/L NaOH solution. The adsorption process was carried out in a thermostat shaker at 220 rpm and 313 K for 24 h to allow equilibrium to be reached. After this time, the suspension was filtered and the dye concentration in the filtrate was analyzed by UV-Visible Spectrophotometer (UV-Vis). The dye adsorption by PTCS (i.e., the adsorption capacity, q_e (mg/g)) and the removal efficiency (R%) were calculated according to Eqs. (1) and (2): [7] [22]

$$q_e = \frac{\left(C_0 - C_e\right)V}{m} \tag{1}$$

$$R\% = \frac{C_0 - C_e}{C_0} \times 100\% \tag{2}$$

where m is the weight of the dry PTCS adsorbent employed (g), V is the solution volume (L), C_0 is the initial dye concentration, and C_e is the equilibrium concentration.

2.4. Effect of PTCS dosage on the adsorption capacity

Five adsorbent dosages (i.e., 15, 20, 25, 30, and 35 mg) were employed to determine the optimum adsorption capacities of PTCS toward initial MB, MO, and RB concentrations of 10, 10, and 5 mg/L, respectively. All adsorption experiments were performed in a thermostatic shaker under the optimal pH values (10 for MB, 4 for MO, and 5 for and RB) at 220 rpm and 313 K for 12 h. After, adsorption equilibrium had been reached, all samples were filtered prior to analysis. The adsorption capacities and removal efficiency (*R*%) were calculated according to Eqs. (1) and (2).

2.5. Adsorption isothermal studies

Isothermal studies were carried out by shaking the adsorbent (15 mg) with solutions of MB, MO, or RB (100 mL) at concentrations ranging from 5 to 35 mg/L and at the optimal pH value for each solution. The adsorption process was conducted with constant stirring at 313 K over 3 h. After this time, the samples were filtered and the concentration of MB, MO or RB in the filtrate was determined by UV-Vis spectrometry. The adsorption capacities and removal efficiency (*R*%) were calculated according to Eqs. (1) and (2).

2.6. Adsorption kinetics

The adsorption kinetics experiments were conducted by shaking a mixture of the adsorbent (15 mg) and a solution of the desired dye (100 mL, 10 mg/L MB, 10 mg/L MO, or 5 mg/L RB) at the optimal pH. The adsorption process was conducted under constant stirring at 313 K, and during this process, the dye concentration in the filtrate was determined by UV-Vis spectrometry at regular time intervals. The adsorption capacities and removal efficiencies (*R*%) were calculated according to Eqs. (1) and (2).

2.7. Characterization of the PTCS adsorbent

The morphological and surface structures of the prepared PTCS adsorbent were characterized by SEM and XPS. The FT-IR spectra of PTCS were recorded on a TENSOR-27 FTIR spectrophotometer.

2.8. Simulated wastewater treatment

Simulated wastewater treatment was carried out by exposing the adsorbent (100 mg) to the mixed simulated pollutant solution (i.e., 100 mL containing MB, MO, RB, Cd^{2+}, and Cr^{3+}, 100 mg/L) for 5 h. The equilibrium concentrations of the dyes and metal ions were determined by UV-Vis and atomic absorption spectroscopy (AAS), respectively. The adsorption capacities and removal efficiencies were calculated according to Eqs. (1) and (2).

2.9. Recyclability of the PTCS bio-adsorbent

The recyclability of the PTCS was determined by mixing the adsorbent (20 mg) with MB (100 mL, 35 mg/L), MO (100 mL, 35 mg/L), or RB (100 mL, 35 mg/L), all dye solutions were prepared with ultra-pure water. Following completion of the adsorption experiment, the PTCS was subjected to centrifugation, immersed in a 60% HCl solution (10 mL) for 5 h, then washed with ultrapure water (×5). The regenerated PTCS was employed in the subsequent adsorption experiment, and this process was repeated five times. The concentrations of the dye compound were determined by UV-Vis spectroscopy.

3. Results and discussion

3.1. Effect of pH on the adsorption capacity

The pH of the adsorption solution not only affects the dye chemical speciation, but also influences the surface charges on the adsorbent [23]. We therefore began to investigate the effect of pH on the adsorption of MB, MO, and RB by PTCS. As indicated in Fig. 1(a), at pH values <7, the removal efficiency of MB by PTCS increased, although no changes were observed above pH 7. In the case of RB, at pH values <10, the removal efficiency was relatively constant, although it dropped significantly at higher pH values. In addition, for the adsorption of MO by PTCS, the removal efficiency increased below pH 4, although the adsorption capacity dropped at higher pH values. The optimal solution pH values for the adsorption of MB, RB, and MO by PTCS were thus determined to be 7, 10, and 4, respectively.

This pH dependence can be attributed to the electrostatic interactions between the PTCS surface groups and the dye molecules, and also to dispersive interactions between the PTCS surface layers and the dye molecules [24]. As the number of H^+ ions increases (i.e., at lower pH values), the amino groups will be protonated to give $-NH_3^+$ moieties on the PTCS surface, which forms strong electrostatic interactions

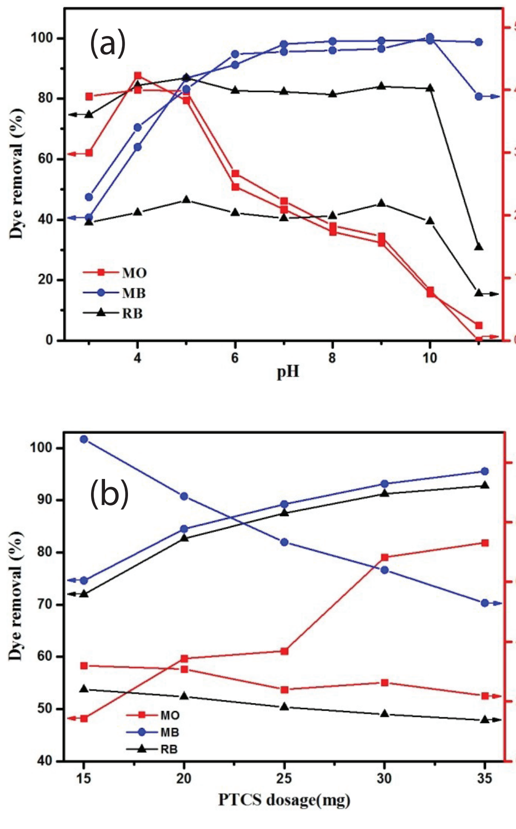

Fig. 1. (a) Effect of pH on the adsorption of MB, MO and RB. (b) The effect of adsorbent dosage on the adsorption of MB, MO and RB.

with anionic dyes such as MO [25]. In contrast, MB is a cationic dye, and the PTCS surface is negatively charged at high pH values, thereby resulting in an increased adsorption rate for MB [26]. Furthermore, RB is a carboxylate-containing basic cationic dye [27], and so good adsorption properties are exhibited by PTCS under either high or low pH values. These results indicated that the surface potential active sites of PTCS are of particular importance when considering dye adsorption.

3.2. Effect of PTCS dosage on the adsorption capacity

The adsorbent dosage has also been demonstrated to be important to determining the adsorption capacity of a material [28]. Thus, Fig. 1(b), shows the adsorption capacity of PTCS toward MB, MO, and RB at different adsorbent dosages. As indicated, upon increasing the PTCS dosage, the adsorption capacity of PTCS increased for all three dyes. This could be attributed to the increased PTCS dosage providing greater numbers of active sites for adsorption. However, with PTCS dosages >30 mg, adsorbent stacking took place, and the adsorption capacity tended to regulate.

3.3. Adsorption isotherm studies

Adsorption isotherm studies can provide information about the adsorbent surface properties, and interactions between an adsorbate and an adsorbent [29–30]. Thus, as shown in Fig. 2(a), which indicated the effect of initial dye concentrations of 5–35 mg/L at 313 K, the optimal adsorption capacities for MB, MO, and RB were 163, 56, and 77 mg/g at initial dye concentrations of 35, 10, and 35 mg/L, respectively. For the adsorption isotherm calculations, the general forms of the Langmuir [30], Freundlich [31], and Temkin [32] models could be expressed as outlined in Eqs. (3), (4), and (5).

$$\frac{C_e}{q_e} = \frac{C_e}{q_{\max}} + \frac{1}{K_L q_{\max}} \tag{3}$$

$$\text{In}q_e = \text{In}K_F + \frac{1}{n}\text{In}C_e \tag{4}$$

$$q_e = B\text{In}K_T + B\text{In}C_e \tag{5}$$

where C_e (mg/L) is the equilibrium concentration, q_e (mg/g) is the quantity of adsorbed metal ions at equilibrium, K_L (L/mg) is the Langmuir model constant, and $q_{\max}$ is the maximum adsorption capacity (mg/g). In addition, K_F (mg/g) (L/g)^n and $1/n$ are the Freundlich isotherm constants.

The adsorption equilibrium data were fitted with the Langmuir, Freundlich, and Temkin isotherm models for a comparative study of the sorption behavior at 313 K, and the results were shown in Figs. 2(b), 2(c), and 2(d). The various isotherm constants and correlation coefficients (R^2) were summarized in Table 1. The isotherm constants were determined from linear isotherm graphs for each of

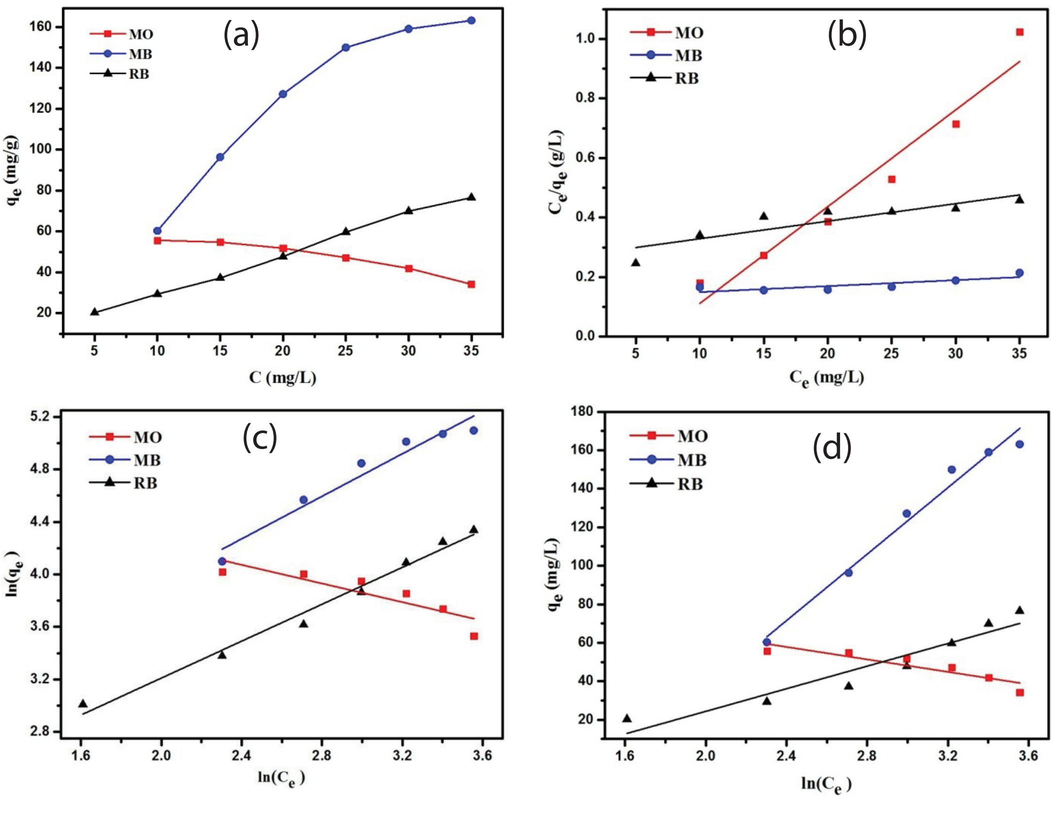

Fig. 2. (a) The effect of initial concentration on the adsorption of MB, MO and RB. The fitting results of the experimental data in terms of Langmuir, (b) Freundlich, (c) Temkin models, and (d) for the adsorption of MB, MO and RB.

the isotherm equations and the correlation coefficient (R^2) was used as a measure of the goodness of isotherm fitting. As indicated in Table 1, the Langmuir isotherm model was suitable for MO, as a correlation coefficient (R^2) of 0.9377 was calculated, which is higher than those obtained for the other two isotherm models. In contrast, the Freundlich isotherm model was applicable to MB (R^2 of 0.9369) and RB (R^2 of 0.9812). It should be noted here that the Freundlich model is widely employed to describe adsorption taking place on a heterogeneous surface, while for the Langmuir model, it is assumed that adsorption occurs on the homogeneous monolayer surface. According to the adsorption isotherm studies, PTCS adsorption of MB and RB occurred not only on the surface of PTCS, but also in the inner pores of PTCS. While, PTCS adsorption of MO occurred just adsorption on the surface of the PTCS. The results can further explain the phenomenon that the adsorption rate of MB and RB by PTCS was higher than MO in the study of pH value and adsorption dosage.

3.4. Adsorption kinetics

The kinetics of dye adsorption is an important parameter in the design of an adsorption process, as it can explain the reaction pathway and the rate-controlling mechanism [33]. Thus, we investigated the effect of contact time on the adsorption of initial MB, MO, and RB concentrations of 10, 10, and 5 mg/L, respectively. As shown in Fig. 3(a), the adsorption capacities for all dyes increased with increasing contact time. A number of kinetic models were used to analyze the adsorption kinetics including the pseudo-first order (Eq. (6)), pseudo-second-order (Eq. (7)), and intraparticle diffusion models (Eq. (8)), which can be expressed as follows [34]:

$$\text{In}(q_e - q_t) = \text{In}q_e - K_1 t \tag{6}$$

$$\frac{t}{q_t} = \frac{1}{K_2 q_e^2} + \frac{t}{q_e} \tag{7}$$

Table 1
Freundlich, Langmuir and Temkin model parameters for the adsorption of MB, MO, and RB onto PTCS

Dye	Langmuir			Freundich			Temkin			Experimental value
	$q_{\max}$ (mg/g)	K_L (L/mg)	R_L^2	n	K_F (mg/g) (mg/L)$^{1/n}$	R_F^2	B (J/mol)	K_T (L/g)	R_T^2	q (mg/g)
MO	130.77	0.1523	0.9377	2.82	137.59	0.7190	–16.17	2.53×10^{-3}	0.7754	60.01
MB	497.51	0.0155	0.6039	1.23	10.25	0.9369	86.39	0.21	0.9365	173.04
RB	169.78	0.0218	0.7438	1.42	6.08	0.9812	29.39	0.31	0.8964	71.06

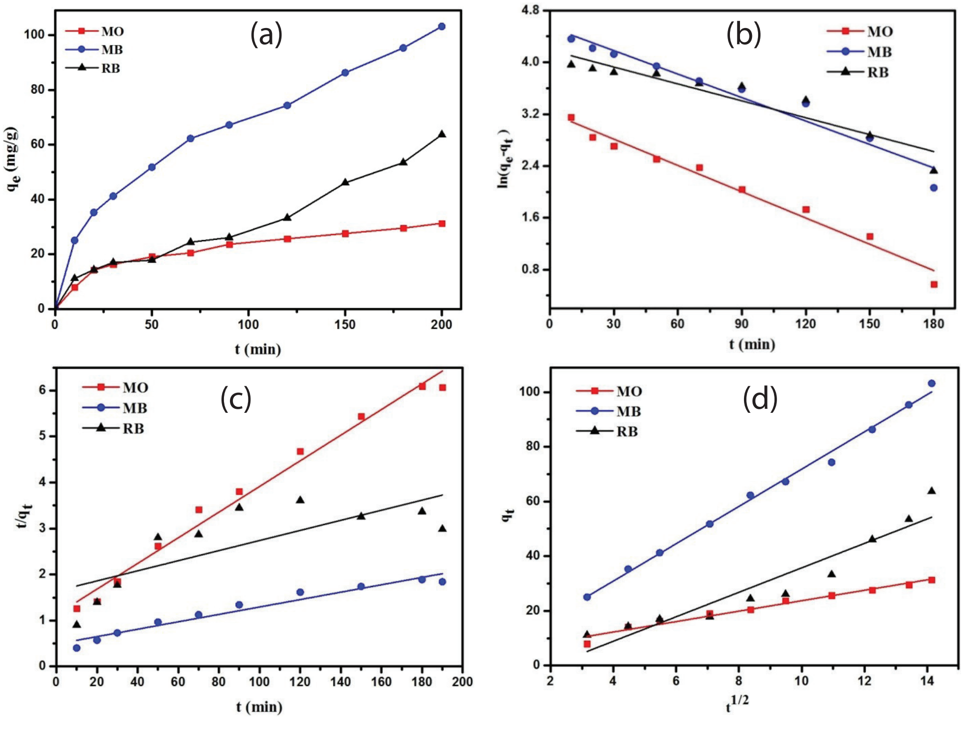

Fig. 3. (a) The effect of contact time on the adsorption of MB, MO and RB. The linear fitting with pseudo-first-order, (b) pseudo-second-order, (c) intraparticle diffusion model, and (d) of the adsorption of MB, MO and RB.

$$q_t = K_i t^{1/2} + C \tag{8}$$

where q_t (mg/g) denotes the adsorption capacity at time t (min), and q_e (mg/g) is the adsorption capacity at equilibrium. In addition, k_1 (1 min^{-1}) is the pseudo-first order adsorption rate constant, k_2 (g/(mg min)) is the pseudo-second-order adsorption rate constant, and k_i (mg/g min$^{1/2}$) is the intraparticle diffusion rate constant.

Figs 3(b), 3(c), and 3(d), showed the pseudo-first order, pseudo-second order, and intraparticle diffusion models, respectively. The kinetic parameters for the adsorption of MB, MO, and RB were summarized in Table 2. The kinetic parameters were determined from linear kinetic graphs for each of the kinetic equations. The correlation coefficient (R^2) is used as a measure of the goodness of kinetic fitting. For the adsorption of MB and MO, the correlation coefficients (R^2) for the pseudo-second-order kinetic model were 0.9838 and 0.9485, which higher than those of the other kinetic models, and the calculated q_e values were similar to the experimental values. These results indicated that the adsorption of MB and MO fit the pseudo-second-order kinetic model, thereby suggesting that these processes mainly involved chemical adsorption [35]. In contrast, the RB adsorption process fits well with the pseudo-first order kinetic model, the correlation coefficients (R^2) for the pseudo-first order kinetic model was 0.8754, which higher than those of the other kinetic models, which indicating that the adsorption of RB mainly took place through physical absorption.

According to the adsorption isotherm and kinetic studies, we can speculate that the adsorption mechanism of the adsorption of MO, MB, RB onto PTCS was mainly electrostatic interaction, π-π interactions and physical adsorption. The adsorption of MO, MB onto PTCS could mainly occur by molecular level interactions among PTCS phenolic hydroxyl groups, amino group, and dye molecules. The adsorption of RB onto PTCS could mainly occur by pore penetration. In addition, there are π-π interactions between the aromatic rings of PTCS and MO, MB, and RB. These adsorption mechanisms allow the dye to be successfully adsorbed on PTCS.

3.5. Characterization of the PTCS bio-adsorbent before and after dye adsorption

The surface morphologies of the PTCS bio-adsorbent before and after dye adsorption were characterized by SEM. As shown in Figs. 4(a)–4(d), the PTCS exhibited an irregular surface and a porous structure, both of which increase the number of available absorption sites, thereby significantly improved the adsorption properties of PTCS toward the dye [33,36]. Following adsorption, numerous small dye particles were observed on the adsorbent, confirming the efficient adsorption of the three dyes by PTCS.

FT-IR spectroscopy was then employed to examine the surface functional groups present on PTCS both before and after adsorption. As shown in Fig. 5(a), the strong and broad peaks at 3,413, 3,420, 3,417, and 3,423 cm^{-1} observed for all four samples (i.e., PTCS and PTCS following the adsorption of the three dye molecules) were attributed to the stretching vibrations of the hydroxyl groups. While the peaks at 2,936, 2,935, 2,930, and 2,933 cm^{-1} were assigned to the C–H stretching vibrations. In the case of PTCS (Fig. 5(a), curve a), the peak at 1,649 cm^{-1} was ascribed to the N-H bending stretching vibration, while those at 1,626, 1,542, 1,454, and 1,321 cm^{-1} were attributed to the ketone C=O stretching vibration, the ring C–C stretching vibration (both 1,542 and 1,454 cm^{-1}), and the O–H bending vibration [37]. Following the adsorption of MB (Fig. 5(a), curve b), the peak at 1,649 cm^{-1} was ascribed to the N-H bending stretching vibration, while that at 1,601 cm^{-1} originated from the ketone C=O stretching vibration. In the case of MO adsorption (Fig. 5(a), curve c), the peaks at 1,606 and 1,313 cm^{-1} were attributed to the ketone C=O stretching vibration and the O–H bending vibration [38]. In addition, following RB adsorption (Fig. 5(a), curve d), the peaks at 1,679, 1,649, and 1,595 cm^{-1} were assumed to originate from the stretching vibrations of the –C=O groups, the N-H bending stretching vibration, and the ketone C=O stretching vibration, respectively [39]. Upon comparison with the pure PTCS spectrum (Fig. 5(a), curve a), the characteristic peak at 1,649 cm^{-1} corresponding to the N–H bending stretching vibration essentially disappeared (Fig. 5(a), curve c), likely due to electrostatic interactions between the amino group and the functional groups on the MO molecule. In addition, a shift in the signal of the ketone C=O stretching vibration from 1,626 to 1,601, 1,606, and 1,595 cm^{-1} following adsorption of the various dyes indicated the presence of π-π interactions between the PTCS and the dye molecules. Furthermore, in the case of MB and RB adsorption, the characteristic peak corresponding to the O-H bending vibration essentially disappeared (Fig. 5(a), curves b and d), likely due to electrostatic bonding between the hydroxyl groups in PTCS and the functional groups of MB and RB.

The results of XPS analysis were shown in Fig. 5(b), the new appearance of S2p (163.87 and 163.94 eV) signal (Fig. 5(b) curves c and d) indicated that the successful adsorption of MB and MO by PTCS. Moreover, the C, O, and N peak

Table 2
Adsorption kinetic parameters for the adsorption of MB, MO, and RB onto PTCS

Dye	Pseudo-first-order equation			Pseudo-second-order equation			Intraparticle-diffusion equation			Experimental value
	$q_{e,\text{cal.1}}$ (mg/g)	K_1	R_f^2	$q_{e,\text{cal 2}}$ (mg/g)	K_2	R_s^2	C	K_i (mg/g min$^{1/2}$)	R_i^2	q_e (mg/g)
MO	41.62	0.0135	0.9744	35.84	6.93×10^{-4}	0.9838	4.62	1.91	0.9716	34.2
MB	114.07	0.0121	0.9463	103.07	1.33×10^{-4}	0.9485	3.64	6.82	0.9342	101.24
RB	67.93	0.0087	0.8754	82.04	7.35×10^{-5}	0.5409	–8.99	4.47	0.8709	52.3

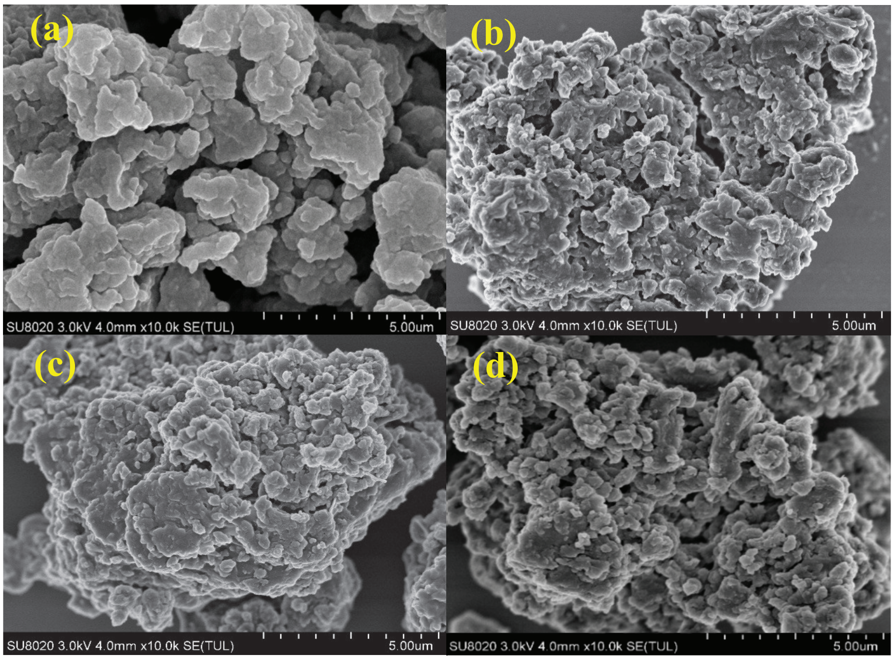

Fig. 4. (a) SEM image of the PTCS, (b) SEM image of the PTCS adsorption MB, (c) SEM image of the PTCS adsorption MO, and (d) SEM image of the PTCS adsorption RB.

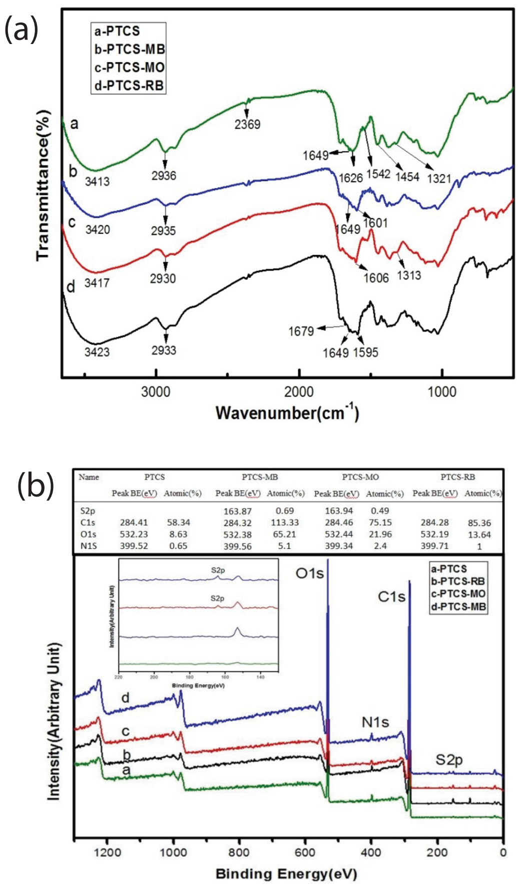

Name	PTCS		PTCS-MB		PTCS-MO		PTCS-RB	
	Peak BE(eV)	Atomic(%)	Peak BE(eV)	Atomic(%)	Peak BE(eV)	Atomic(%)	Peak BE(eV)	Atomic(%)
S2p			163.87	0.69	163.94	0.49		
C1s	284.41	58.34	284.32	113.33	284.46	75.15	284.28	85.36
O1s	532.23	8.63	532.38	65.21	532.44	21.96	532.19	13.64
N1S	399.52	0.65	399.56	5.1	399.34	2.4	399.71	1

Fig. 5. (a) FTIR spectra of PTCS, PTCS adsorption MB, PTCS adsorption MO, PTCS adsorption RB, (b) XPS of PTCS, PTCS adsorption MB, PTCS adsorption MO, PTCS adsorption RB.

intensities increased as the adsorption of MO, MB, RB onto PTCS (Fig. 5(b), curves a, b, and c), indicating the adsorption of PTCS on dye was confirmed.

3.6. Simulated wastewater treatment

To estimate the adsorption performance of PTCS toward sewage, we conducted simulated wastewater treatment experimentsusing MB, MO, RB, Cd^{2+}, and Cr^{3+} [40], and the results are shown in Fig. 6(a). The contaminant removal efficiency for MB, MO, RB, Cd^{2+}, and Cr^{3+} were 72%, 59%, 63%, 54%, and 52%, respectively. Interestingly, the adsorption capacities for the dyes were higher than those of the metal ions, which are likely due to the dye adsorption mechanism consisting of more than simply electrostatic interactions, which dominate in the case of metal ions.

3.7. Recyclability of PTCS

In industrial applications, recyclability and reproducibility are necessary parameters for evaluating the stability of an adsorbent and its potential application. Fig. 6(b), shows the results obtained upon recycling PTCS for the adsorption of MB, MO, and RB. As shown in Fig. 6(b), the removal efficiency of MB in the repeated use did not decrease significantly. After 6 cycles of usage, the removal efficiency remained 83%. While for MO and RB, the the removal efficiency changed from 46% to 35%, and from 54% to 47%.

The removal efficiency for MB was higher compared with other pollutants after 6 cycles of usage. This was maybe the recycling experiments was conducted in neutral solution. When the pH was neutral, the amino group protonation on the surface of PTCS was decreased, and leaded to the positive charge on the surface of PTCS was reduced, so the removal

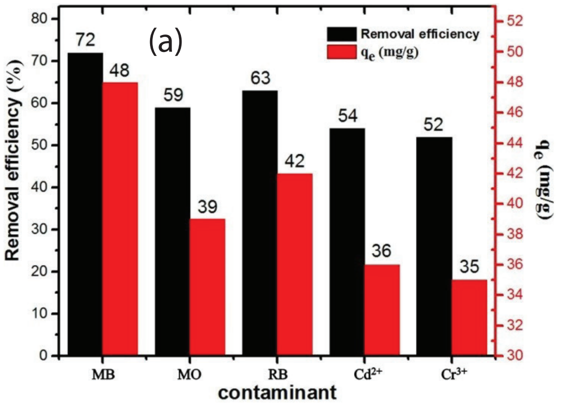

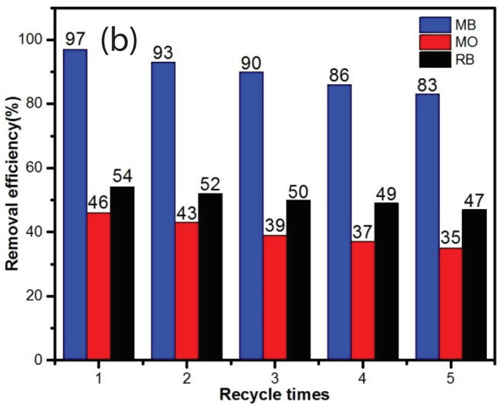

Fig. 6. (a), Simulation experiment of the PTCS adsorption of pollutant, (b) The recyclability of PTCS adsorption MB, MO and RB.

efficiency of PTCS on MO was decreased. At the same time, when pH is neutral, the carboxyl group of RB and hydroxide in the surface of PTCS were mutually exclusive, so the removal efficiency of PTCS on RB was lower. Therefore, the removal efficiency for MB was higher compared with MO and RB. These results indicated that PTCS is a stable adsorbent that can be readily recycled, and so could potentially be employed for a range of practical applications.

4. Conclusions

We herein reported the preparation of a low cost and environmentally friendly adsorbent (PTCS) through the functionalization of PT with CS. The prepared PTCS exhibited a high adsorption capacity for MB,MO, and RB dyes in aqueous media. Adsorption experiments confirmed that the adsorption of MB, MO, RB, onto PTCS was highly dependent on pH, bio-adsorbent dosage, initial dyes concentration. The maximum adsorption capacity of MB, MO, RB was 173.04, 60.01, 71.06 mg/g at 313 K and pH 7, 4, 10, respectively. In addition, the Langmuir isotherm model was more suitable for the adsorption of MO onto PTCS, while the Freundlich isotherm model was applicable for the adsorption of MB and RB. Furthermore, the kinetic studies showed that the adsorption data obtained for MB and MO correlated with the pseudo-second-order model, while the adsorption of RB fitted well with the pseudo-first-order model. A possible mechanism for the adsorption of MB, MO, RB, onto PTCS was proposed, where electrostatic interactions, π-π interactions and physical adsorption dominated. These results indicate that PTCS may be used as a highly adaptable adsorbent for removing cationic, anionic dyes from wastewater.

Acknowledgments

This work was supported by the National Nature Science Foundation of China (grant numbers 81760451 and 51471055), the National Science Foundations of Guangxi province of China (grant numbers 2016GXNSFGA380001 and 2016GXNSFAA380080). We would like to thank Editage [www.editage.cn] for English language editing.

Conflict of interest

The authors declare that they have no conflict of interest.

References

[1] S. Sohni, K. Gul, F. Ahmad, I. Ahmad, A. Khan, N. Khan, S. B. Khan, Highly efficient removal of acid red-17 and bromophenol blue dyes from industrial wastewater using graphene oxide functionalized magnetic chitosan composite, Polymer Comp., 39 (2018) 3317–3328.

[2] M. Tanzifi, S.H. Hosseini, A.D. Kiadehi, M. Olazar, k. Karimipour, R. Rezaiemehr, I. Ali, Artificial neural network optimization for methyl orange adsorption onto polyaniline nano-adsorbent: kinetic, isotherm and thermodynamic studies, J. Molec. Liq., 244 (2017) 189–200.

[3] S. Pu, S. Xue, Z. Yang, Y.Q. Hou, R.X. Zhu, W. Chu, In situ co-precipitation preparation of a superparamagnetic graphene oxide/Fe_3O_4, nanocomposite as an adsorbent for wastewater purification: synthesis, characterization, kinetics, and isotherm studies, Environ. Sci. Pollut. Res., 25 (2018) 17310–17320.

[4] M.S.T. Gonçalves, A.M.F. Oliveira-Campos, E.M.M.S. Pinto, M.S.P. Paula, Queiroz mjrp, Photochemical treatment of solutions of azo dyes containing TiO_2, Chemosphere., 39 (1999) 781–786.

[5] C. Belpaire, T. Reyns, C. Geeraerts, J.V. Loco, Toxic textile dyes accumulate in wild European eel Anguilla anguilla, Chemosphere., 138 (2015) 784–791.

[6] R. Jain, M. Mathur, S. Sikarwar, A. Mittal, Removal of the hazardous dye rhodamine B through photocatalytic and adsorption treatments, J. Environ. Manage., 85 (2007) 956–964.

[7] M. Gurung, B.B. Adhikari, K. Khunathai, H. Kawakita, K. Ohto, H. Harada, K. Inoue, Quaternary amine modified persimmon tannin gel: an efficient adsorbent for the recovery of precious metals from hydrochloric acid media, Separ. Sci. Technol., 46 (2011) 2250–2259.

[8] J. Cui, Z.M. Wang, F.L. Liu, P.B. Dai, R. Chen, H.Y. Zhou, Preparation of persimmon tannins immobilized on collagen adsorbent and research on its adsorption to Cr(VI), Mater. Sci. Forum., 744 (2013) 523–530.

[9] N. Abidi, E. Errais, J. Duplay, A. Berez, A. Jrad, G. Schaefer, M. Ghazi, K. Semhi, M. Trabelsi-Ayadi, Treatment of dye-containing effluent by natural clay, J. Cleaner Prod., 86 (2015) 432–440.

[10] R. Ahmad, R. Kumar, Adsorptive removal of congo red dye from aqueous solution using bael shell carbon, Appl. Surface Sci., 257 (2010) 1628–1633.

[11] A. Akbari, J.C. Remigy, P. Aptel, Treatment of textile dye effluent using a polyamide-based nanofiltration membrane, Chem. Eng. Process. Process Intensif., 41 (2002) 601–609.

[12] Z. Zhou, F. Liu, Y. Huang, Z.M. Wang, G.Y. Li, Biosorption of palladium(II) from aqueous solution by grafting chitosan on persimmon tannin extract, International J. Bio. Macromol., 77 (2015) 336–343.

[13] Z. Wang, X. Li, H. Liang, J.L. Ning, Z.D. Zhou, G.Y. Li, Equilibrium, kinetics and mechanism of Au^{3+}, Pd^{2+}, and Ag^{+}, ions adsorption from aqueous solutions by graphene oxide functionalized persimmon tannin, Mater. Sci. Eng. C., 79 (2017) 227–236.

[14] X.J. Li, Z.M. Wang, J.L. Ning, M.M. Gao, W.B. Jiang, Z.D. Zhou, G.Y. Li, Preparation and characterization of a novel polyethyleneimine cation-modified persimmon tannin bioadsorbent for anionic dye adsorption, J. Environ. Manage., 217 (2018) 305–314.

[15] F.L. Liu, Z.M. Wang, J. Cui, Z.D. Zhou, G.Y. Li, H.Y. Zhou, Adsorption for Au^{3+} by persimmon tannins immobilized on collagen fiber, Mater. Sci. Forum., 745 (2013) 39–45.

[16] Y.H. Chang, C.F. Huang, W.J. Hsu, F.C. Chang, Removal of Hg^{2+} from aqueous solution using alginate gel containing chitosan, J. Appl. Polym. Sci., 104 (2007) 2896–2905.

[17] A. Roy, B. Adhikari, S.B. Majumder, Equilibrium, kinetic, and thermodynamic studies of azo dye adsorption from aqueous solution by chemically modified lignocellulosic jute fiber, Ind. Eng. Chem. Res., 52 (2013) 6502–6512.

[18] G. Crini, P.M. Badot, Application of chitosan, a natural aminopolysaccharide, for dye removal from aqueous solutions by adsorption processes using batch studies: a review of recent literature, Progr. Polym. Sci., 33 (2008) 399–447.

[19] X. Xu, X.Y. Jiang, F.P. Jiao, X.Q. Chen, J.G. Yu, Tunable assembly of porous three-dimensional graphene oxide-corn zein composites with strong mechanical properties for adsorption of rare earth elements, J. Taiwan Inst. Chem. Eng., 85 (2018) 106–114.

[20] J.Y. Yang, X.Y. Jiang, F.P. Jiao, J.G. Yu, The oxygen-rich pentaerythritol modified multi-walled carbon nanotube as an efficient adsorbent for aqueous removal of alizarin yellow R and alizarin red S, Appl. Surf. Sci, 436 (2018) 198–206.

[21] J. Teng, X. Zeng, X. Xu, J.G. Yu, Assembly of a novel porous 3D graphene oxide-Starch architecture by a facile hydrothermal method and its adsorption properties toward metal ions, Mater. Lett., 214 (2018) 31–33.

[22] X. Li, Z. Wang, H. Liang, J.L. Ning, G.Y. Li, Z.D. Zhou, Chitosan modification persimmon tannin bioadsorbent for highly efficient removal of Pb(II) from aqueous environment: the adsorption equilibrium, kinetics and thermodynamics, Environ. Technol., 40 (2019) 112–124.

[23] A.L. Martins, L.A. Teixeira, F.V. Fonseca, L. Yokoyama, Evaluation of the mercaptobenzothiazole degradation by combined adsorption process and Fenton reaction using iron mining residue, Environ. Technol., 38 (2016) 1–8.

[24] M. Arshadi, F. Mousavinia, M.J. Amiri, A.R. Faraji, Adsorption of methyl orange and salicylic acid on a nano-transition metal composite: kinetics, thermodynamic and electrochemical studies, J. Colloid Interface Sci., 483 (2016) 118–131.

[25] Y. Wang, Y. Xie, Y. Zhang, S.Y. Tang, C.C. Guo, J.S. Wu, R. Lau, Anionic and cationic dyes adsorption on porous poly-melamine-formaldehyde polymer, Chem. Eng. Res. Design., 114 (2016) 258–267.

[26] L. Chen, Y.H. Li, S. Hu, J.K. Sun, Q.J. Du, X.X. Yang, Q. Ji, Z.H. Wang, D.C. Wang, Y.Z. Xia, Removal of methylene blue from water by cellulose/graphene oxide fibres, J. Experim. Nanosci., 11 (2016) 1–15.

[27] L. Li, S. Liu, T. Zhu, Application of activated carbon derived from scrap tires for adsorption of Rhodamine B, J. Environ. Sci., 22 (2010) 1273–1280.

[28] R. Tabaraki, S. Ahmady-Asbchin, O. Abdi, Biosorption of Zn(II) from aqueous solutions by Acinetobacter, sp. isolated from petroleum spilled soil, J. Environ. Chem. Eng., 1 (2013) 604–608.

[29] L. Wang, C. Mao, N. Sui, M.H. Liu, W.Yu, Graphene oxide/ferroferric oxide/polyethylenimine nanocomposites for Congo Red adsorption from water, Environ. Technol., 38 (2016) 996–1004.

[30] D. Yang, L. Qiu, Y. Yang, Efficient adsorption of methyl orange using a modified chitosan magnetic composite adsorbent, J. Chem. Eng. Data., 61 (2016) 3933–3940.

[31] M.Y. Chang, R.S. Juang, Adsorption of tannic acid, humic acid, and dyes from water using the composite of chitosan and activated clay, J. Colloid Interface Sci., 278 (2004) 18–25.

[32] L.P. Lingamdinne, J.R. Koduru, Y.L. Choi, Y.Y. Chang, Studies on removal of Pb(II) and Cr(III) using graphene oxide based inverse spinel nickel ferrite nano-composite as sorbent, Hydrometallurgy., 165 (2016) 64–72.

[33] M. Rafatullah, O. Sulaiman, R. Hashim, A. Ahmad, Adsorption of methylene blue on low-cost adsorbents: a review, J. Hazard. Mater., 177 (2010) 70–80.

[34] L. Li, Z. Wang, P. Ma, H.Y. Bai, W.F. Dong, M.Q. Chen, Preparation of polyvinyl alcohol/chitosan hydrogel compounded with graphene oxide to enhance the adsorption properties for Cu(II) in aqueous solution, J. Polym. Res., 22 (2015) 150–156.

[35] J. Zhou, C. Tang, B. Cheng, J.G. Yu, M. Jaroniec, Rattle-type carbon-alumina core-shell spheres: synthesis and application for adsorption of organic dyes, ACS Appl Mater Interfaces., 4 (2012) 2174–2179.

[36] Z.H. Wang, J.Y. Yang, X.W. Wu, X.Q. Chen, J.G. Yu, Y.P. Wu, Enhanced electrochemical performance of porous activated carbon by forming composite with graphene as high-performance supercapacitor electrode material, J. Nanopart. Res., 19 (2017) 77–82.

[37] J. Sánchez-Martín, M. González-Velasco, J. Beltrán-Heredia, J. Gragera-Carvajal,J. Salguero-Fernández, Novel tannin-based adsorbent in removing cationic dye (Methylene Blue) from aqueous solution: kinetics and equilibrium studies, J. Hazard. Mater., 174 (2010) 9–16.

[38] M. Gurung, B.B. Adhikari, H. Kawakita, K. Ohto, K. Inoue, S. Alam, Selective recovery of precious metals from acidic leach liquor of circuit boards of spent mobile phones using chemically modified persimmon tannin gel, Ind. Eng. Chem. Res., 51 (2012) 11901–11905.

[39] Y. Jing, H. Gao, C. Yang, Chitosan microspheres modified with poly (ethylenimine) enhance the adsorption of methyl orange from aqueous solutions, Asia-Pacific J. Chem. Eng., 11 (2016) 428–436.

[40] Z.J. Zhang, L. Zhu, W. Lu, X.F. Li, X.Q. Sun, R.Y. Lü, H.G. Ding, Evaluation of functional group content of N-methylimidazolium anion exchange resin on the adsorption of methyl orange and alizarin red, Chem. Eng. Res. Design., 111 (2016) 161–168.